Extracellular vesicles bearing serum amyloid A1 exacerbate neuroinflammation after intracerebral haemorrhage

Huimin Zhu,[1] Ningning Wang,[1] Yingying Chang,[1,2] Ying Zhang,[3] Shihe Jiang,[3] Xiaoping Ren,[3] Meng Yuan,[3] Haoxiao Chang,[3] Wei-Na Jin [ID] [1,3]

[1]Department of Neurology, Tianjin Neurological Institute, Tianjin Medical University General Hospital, Tianjin, China
[2]The Third Affiliated Hospital of Zhengzhou University, Zhengzhou, Henan, China
[3]China National Clinical Research Center for Neurological Diseases, Beijing Tiantan Hospital, Beijing, China

Correspondence to
Dr Wei-Na Jin;
weina.jin@ncrcnd.org.cn

ABSTRACT

Introduction Intracerebral haemorrhage (ICH) elicits a robust inflammatory response, which significantly contributes to secondary brain damage. Extracellular vesicles (EVs) play a pivotal role in intercellular communication by transporting immune-regulatory proteins. However, the precise contribution of these EV-carried proteins to neuroinflammation following ICH remains elusive. Here, we identified proteins dysregulated in EVs and further studied the EVs-enriched Serum amyloid A 1 (SAA1) to understand its role in neuroinflammation and ICH injury.

Methods We used mass spectrometry to analyse the EV protein cargo isolated from plasma samples of 30 ICH patients and 30 healthy controls. To validate the function of the dysregulated protein SAA1, an ICH mouse model was conducted to assess the effects of SAA1 neutralisation on brain oedema, neurological function and infiltration of peripheral leucocytes.

Results 49 upregulated proteins and 12 downregulated proteins were observed in EVs from ICH patients compared with controls. Notably, SAA1 demonstrated a significant increase in EVs associated with ICH. We observed that exogenous SAA1 stimulation led to an augmentation in the population of microglia and astrocytes, exacerbating neuroinflammation. Neutralising SAA1 with an anti-SAA1 monoclonal antibody (mAb) diminished the prevalence of proinflammatory microglia and the infiltration of peripheral leucocytes, which ameliorates brain oedema and neurological function in ICH mice.

Conclusion Our findings provide compelling evidence implicating EVs and their cargo proteins in ICH pathogenesis. SAA1 emerges as a potential therapeutic target for mitigating neuroinjury and neuroinflammation following ICH.

INTRODUCTION

Intracerebral haemorrhage (ICH) stands as a devastating disease, constituting 15%–20% of all strokes, yet bearing a high mortality rate.[1 2] Despite its prevalence, effective treatments for ICH remain limited.[3] During the acute phase, proteins are secreted via various mechanisms including extracellular vesicles (EVs), transporter-mediated processes and passive diffusion.[4] EVs, encompassing exosomes

> **WHAT IS ALREADY KNOWN ON THIS TOPIC**
> ⇒ Intracerebral haemorrhage (ICH) triggers pronounced inflammatory response, which is a major factor in secondary brain damage. Extracellular vesicles (EVs) bridge extracellular communication by transforming immune-regulated proteins.
>
> **WHAT THIS STUDY ADDS**
> ⇒ We identified proteins that are dysregulated in EVs and further studied EVs-enriched Serum amyloid A 1 (SAA1) to understand its role in neuroinflammation and ICH injury.
>
> **HOW THIS STUDY MIGHT AFFECT RESEARCH, PRACTICE OR POLICY**
> ⇒ This study demonstrates that EVs and their bearing proteins contribute to ICH pathogenesis, which suggests that targeting SAA1 may be a potential treatment option to reduce neuroinjury and neuroinflammation after ICH.

and microvesicles, are released by cells into extracellular fluids and serve as conduits for intercellular communication by transporting proteins, metabolites, lipids and nucleic acids to recipient cells.[5–7] Certain proteins and miRNAs encapsulated within EVs have shown promise as biomarkers for assessing the risk and prognosis of ICH.[8 9]

The overall impact of EVs manifests a dual role in the context of ICH.[8] Previous studies have demonstrated that inhibiting EV release exacerbates neuroinflammation, whereas administration of EVs derived from ICH patients and mice promotes recovery.[9 10] Conversely, some miRNAs carried by EVs may bind to circulating neutrophils, facilitating their transendothelial migration into the brain.[11] Consequently, the net effect of EVs on brain injury remains inconclusive. To elucidate the mechanisms underlying EV action, the protein content of blood-derived EVs was examined via proteomics in an ICH mouse model.[12] The findings revealed that a majority

of these proteins are associated with cellular damage, deubiquitylation, regulation of MAP kinase activity and signal transduction.

On neuroinflammation onset, EVs serve as vehicles for transporting proteins across the blood–brain barrier (BBB), potentially exerting either anti-inflammatory or proinflammatory effects in response to central nervous system damage. Proinflammatory cytokines such as IL-1β, IFN-γ, TNF-α and caspase-1 can be encapsulated within these vesicles and contribute to an inflammatory microenvironment.[13] Additionally, EVs play a pivotal role in BBB disruption, facilitating the infiltration of CD4+ and CD8+ T lymphocytes and leucocytes into the brain.[14 15] Some evidence suggests protective functions, such as promoting the migration and/or differentiation of oligodendrocyte precursor cells.[16] Thus, EVs exhibit dual roles in neuroinflammation, being potentially detrimental or protective. However, the specific role of EVs carrying proteins and their mechanisms in ICH patients remains unclear.

In this study, we used proteomics to screen for dysregulated proteins in EVs from ICH patients, aiming to identify potential targets for mitigating neuroinflammation following ICH.

METHODS
Patient and public involvement
Patients who previously had ICH and their families were not involved in setting the research question or the outcome measures but were intimately involved during basic information collection. Patients and their families also signed the informed consent and were willing to donate blood samples to our research. Dissemination of baseline information is critical as it helped to motivate community involvement during and beyond the study.

Patients' enrolment
Demographic and clinical characteristics of the ICH patients and controls are presented in table 1. Specifically, 30 patients with ICH (6 females, 24 males) and 30 healthy controls (9 females, 21 males) were included with blood samples collected for EVs isolation and proteomic analysis. Further, samples from another 21 patients with ICH and 15 healthy controls were collected for validation by ELISA (table 1). The blood samples were obtained from ICH patients in both the discovery and validation cohorts within 24 hours post-ICH onset (discovery cohort: median (IQR): 24 (9, 24) hours; validation cohort: median (IQR): 9 (6, 15) hours). Inclusion and exclusion criteria were established for patients diagnosed with ICH. Enrolled participants were required to be 18 years of age or older and have a confirmed intracerebral hematoma detected by CT imaging. Exclusion criteria encompassed concurrent conditions such as tumours, pre-existing brain disorders, infections, autoimmune diseases and ongoing immune-related therapies. CT imaging and NIHSS (National Institutes of Health Stroke Scale, online supplemental table 1) were obtained to evaluate the severity of the patient's condition. Control subjects, also aged 18 years or older, exhibited normal basic laboratory findings. Exclusion criteria for controls included neurological or psychiatric disorders, history of tumours and prior use of medications such as antihypertensives and antidiabetic drugs.

Animals
We performed the mice research following the guidelines of 'Animal Research: Reporting In Vivo Experiments' and 'National Institutes of Health for the Care and Use of Laboratory Animals'. We used healthy male mice aged eight to ten weeks for this investigation. The C57BL/6J

Table 1 Demographic and clinical characteristics of the ICH and the control groups

Discover set for proteomics	ICH group (n=30)	Control group (n=30)	P value
Gender, F/M	6/24	9/21	0.552
Age (year), mean (SEM)	52.1 (2.3)	49.9 (1.9)	0.459
Time points post-ICH (hours), median (IQR)	24 (9, 24)	NA	NA
NIHSS, median (IQR)	13 (11, 19.25)	NA	NA
Haemorrhage volume (mL), median (IQR)	6.8 (4.6, 15.5)	NA	NA
Validation set for ELISA	**ICH group (n=21)**	**Control group (n=15)**	**P value**
Gender, F/M	9/12	3/12	0.282
Age (years), mean (SEM)	61.3 (3.06)	58.8 (3.53)	0.592
Neutrophile ×10^9, mean (SEM)	6.713 (0.952)	NA	NA
Leucocyte ×10^9, mean (SEM)	8.516 (0.937)	NA	NA
Time points post-ICH (hours), median (IQR)	9 (6, 15)	NA	NA
NIHSS, median (IQR)	12 (11, 20)	NA	NA
Haemorrhage volume (mL), median (IQR)	17 (12.5, 36.5)	NA	NA

ICH, intracerebral haemorrhage; NA, not available; NIHSS, National Institute of Health Stroke Scale; SEM, SE of the mean.

mice were obtained from SPF Biotechnology Corporation in Beijing, China. No more than five mice were housed per cage, and pathogen-free environments were maintained with unrestricted access to food and water. Mice were subjected to a 12-hour light-dark cycle. Different groups of mice were randomly placed in cages. A total of 165 mice were used in this study, and 15 mice were excluded due to unsuccessful model induction.

EVs isolation

We isolated EVs from patients and healthy subject plasma using a polymer formulation sedimentation process. The extraction method involved using ExoQuick-TC Exosome Precipitation Solution (EQULTRA-20A-1, System Biosciences, USA) following previously described protocols.[17] Initially, 300 µL of plasma underwent centrifugation twice at 10 000 g for 15 min at 4°C to collect the supernatant. Subsequently, 93 µL of Exosome isolation solution was mixed and incubated on ice for 30 min. Following this, sediment was collected after centrifugation at 3000 for 10 min at 4°C. The addition of 200 µL of solution A and 200 µL of solution B with gentle mixing facilitated rough purification.

Transmission electron microscopy

Transmission electron microscopy (TEM) with negative-contrast staining was used to observe exosomes isolated from the serum of ICH patients. Fresh EV suspensions were mixed with 4% paraformaldehyde (1:1) and adsorbed onto EM grid membranes coated by Formvar/carbon (20–30 min). They were then stained in a solution containing uranyl acetate and methyl cellulose (10 min), and air-dried to facilitate exosomes visualisation via TEM (H-7650, Hitachi, Japan).[18]

Nanoparticle tracking analysis

All EVs were measured using the ZetaView Nanoparticle Tracker (Particle Metrix, Meerbusch, Germany) to check for the inclusion criteria and for calculations. Initially, the instrument was calibrated using polystyrene particles with an approximate size of 100 nm. Following calibration, the EVs were diluted to a concentration of around 1×10^8 particles/mL and introduced into the instrument for analysis. Each sample underwent automatic scanning in nine directions to eliminate any aberrant data points. The final data were recorded and analysed using ZetaView V.8.03.04.01 software.

Western blot analysis

We blocked the membranes with primary antibodies from Abcam (CD63 ab134045, TSG101 ab125011). Detailed methods are provided in online supplemental material.

Label-free quantitative proteomics

We randomly divided 30 EVs into 3 groups per prior literature.[19 20] We used Matrix-Assisted Laser Desorption Ionization Time-Of-Flight Mass Spectrometry (MALDI-TOF-MS/MS) and database searching to identify EV proteins. Detailed methods are provided in online supplemental material.

Biological information analysis

We conducted protein–protein interaction (PPI) network analysis using the free web-based search tool STRING (V.12.0) and depicted using Cytoscape (V.3.9.1).[17] Detailed methods are provided in online supplemental material.

GO analysis and Kyoto Encyclopaedia of Genes and Genomes analysis

GO enrichment analysis was performed to categorise the differentially expressed proteins (DEPs) and their pathways. This enabled us to efficiently examine each protein and understand its relationship with its biological functions. Pathway analysis facilitated the identification of the most significant biochemical-metabolic and signalling pathways within the chosen proteins. For functional annotation of differentially expressed genes, we employed the Kyoto Encyclopaedia of Genes and Genomes (KEGG) database (Release 91.0). The calculated p values underwent false discovery rate (FDR) correction, with FDR<0.05 considered as the threshold. KEGG analysis was performed via the clusterProfiler R package.[21]

ELISA quantification analysis

We identified several proteins that were upregulated, including serum amyloid A component A (SAA1), alpha-enolase 1 (ENO1), thymosin beta 4 (TMSB4X), angiogenin (ANG), FLN-α (filamin-α) and growth factor receptor-bound protein-2 (Grb2). To detect these proteins in both plasma and EVs of patients and subjects, we employed the following ELISA kits: human SAA1 ELISA kit (DY3019-05, R&D, USA), human TMSB4X ELISA kit (EIA-TMSB4X, Raybiotech, USA), human ENO1 ELISA kit (ab181417, Abcam, UK), human Angiogenin ELISA kit (ELH-ANG-5, Raybiotech, USA), human FLN-α ELISA kit (OSD-H1620, OUSAID, China), human Grb2 ELISA kit (OSD-H1509, OUSAID, China) and mouse ELISA kit (CSB-EL020656MO, CUSABIO, China). The ELISA microplates were analysed using a microplate reader (Tecan, SPARK, Switzerland).

Induction of murine ICH model

We induced the ICH model in mice by injecting collagenase as previously described.[22 23] During the stereotaxic injection procedure, mice were anaesthetised using avertin and secured on a stereotactic frame. A 1-mm-diameter hole was drilled on the right side of the skull, 2.3 mm lateral to the midline and 0.5 mm anterior to the bregma. The 0.0375 U bacterial collagenase IV (C8160, Solarbio, China) was dissolved in 1 µL saline and infused into the striatum (3.7 mm deep relative to bregma) at a rate of 0.5 µL/min after the needle was left in the brain for 10 min. Sham controls received an equal volume of saline. After a further 10 min interval to prevent backflow, the needle was gently withdrawn 1 mm and allowed to rest for 5 min before removal from the

brain. The cranial burr hole was sealed with bone wax, and the incision was sutured. Throughout the procedure, the animal's temperature was maintained at 37°C using a homeothermic blanket. Postsurgery animals were kept under observation with unrestricted access to food and water. Penicillin was received at a dose of 1.25 mg/g via subcutaneous infusion once daily.

Exogenous SAA1 intracerebral injection
To evaluate the exogenous effect of SAA1 on the mouse brain, we administered varying doses (0 ng, 83 ng, 250 ng, 750 ng) of SAA1 protein (CSB-EP020656MO, CUSABIO, China) dissolved in 1 µL of saline via intracerebral injection. The stereotaxic injection procedure was identical to that used for the induction of the murine ICH model described above.

Immunostaining and histology
The primary antibodies used were anti-mouse Iba1 (ab178847, Abcam, UK) and anti-mouse GFAP (3670, Cell Signaling Technology, USA). Detailed methods are provided in online supplemental material.

In vivo antibody administration
We used anti-mouse SAA1 mAb (AF2948, NOVUS, USA) to block SAA1 in vivo at a dose of 0.25 µg/g, as previously reported.[24] To establish a control, we administered Goat IgG Isotype Control (AB-108-C, NOVUS, USA). Both the monoclonal antibody and the isotype were injected through the tail vein 1 hour after induction of ICH.

Flow cytometry
We prepared single-cell suspensions for flow cytometry from the brain, following methods previously reported.[22 25] After euthanising mice with avertin anaesthesia, we extracted the brain, minced the tissue and treated it with collagenase I at 37°C for 40 min. Following removal of myelin debris by centrifugation in 30% percoll, we stained single cells with fluorescently conjugated antibodies. For intracellular staining, cells underwent fixation in a buffer for 20 min after surface marker staining. Subsequently, after two washes in permeabilisation buffer, cells were incubated with intracellular antibodies in a staining buffer for 30 min. All flow cytometry antibodies were obtained from Biolegend and included CD45-APC-Cy7 (Cat# 103116), CD11b-PE-Cy7 (Cat# 101216), CD86-APC (Cat# 105012), CD206-FITC (Cat# 141703), F4/80-PE (Cat# 123110), Ly6G-Percp-Cy5.5 (Cat# 127616), CD3-PE (Cat# 100206), CD4-APC (Cat# 100412), CD8-FITC (Cat# 100706), CD19-PE-Cy7 (Cat# 115520) and 7-AAD (Cat# 420404), Annexin V-PE (Cat# 640947). Samples were analysed using FACS Aria (BD Biosciences, USA) and FlowJo software (V.10.8.1).

Neurological function assessment
Two investigators blinded to the treatment groups conducted neurological function assessments. Following recovery from ICH surgery, we employed the modified Neurological Severity Score (mNSS score) (online supplemental table 2) and the rotarod test to assess neurodeficits day 1 and day 3 postsurgery.[22]

1. The modified Neurological Severity Score serves as a comprehensive tool for evaluating motor function (muscle and abnormal movement), sensory function (visual, tactile and proprioceptive) and reflexes (pinna, corneal and startle reflexes). Scores range from 0 to 18 and are delineated as follows: severe injury (13–18), moderate injury (7–12) and mild injury (1–6).[25 26]
2. The rotarod test was employed to gauge motor coordination and balance. Mice underwent 3 days of training prior to surgery and were tested on day 1 and day 3 postsurgery. Placed on a rotating rod with a non-slippery surface, the test began at four rotations per minute (rpm) and accelerated to 40 rpm over 240 s, with a maximum test duration of 10 min. Each mouse underwent three trials with a 15 min interval between each. Results were averaged across the three trials.[27]

Murine neuroimaging
We used the 7.0T small-animal MRI scanner (Clinscan, Bruker, Germany) to assess lesion volume. Detailed methods are provided in online supplemental material.

Statistical analysis
We conducted statistical analyses using GraphPad Prism software (V.8.0.2). Data are expressed as means±SEM. We considered values of $p < 0.05$ as statistically significant. Specific sample sizes (n) are detailed in the figure captions, indicating the number of animals or patient samples used in either in vitro or in vivo experiments. Experimental groups, data collection and data analysis underwent blinding procedures, with different investigators or masked sample labels used. Animal experiments were randomly allocated to experimental groups. Exclusion of samples occurred due to mouse mortality postsurgery. We employed the two-tailed unpaired Student's t-test to ascertain significant differences between two groups. For comparisons among multiple groups, we used one-way analysis of variance, followed by Tukey's test to compare each group individually, and the Kruskal-Wallis test for non-parametric multigroup comparisons. Correlations were assessed using the Pearson correlation coefficient test.

RESULTS
Baseline characteristics of ICH patients
We included a total of 60 patient samples in our study to screen EVs for proteomics analysis. This comprised 30 ICH patients (24 male, 6 female; mean age: 52.1) and 30 controls (21 male, 9 female; mean age: 49.9). Additionally, we included 36 patient samples for validation analysis, consisting of 21 ICH patients (12 male, 9 female; mean age: 61.3) and 15 controls (12 male, 3 female; mean age: 58.8) (table 1). Demographic characteristics showed no statistically significant differences between the ICH and healthy control groups in both the proteomics and validation sets (table 1).
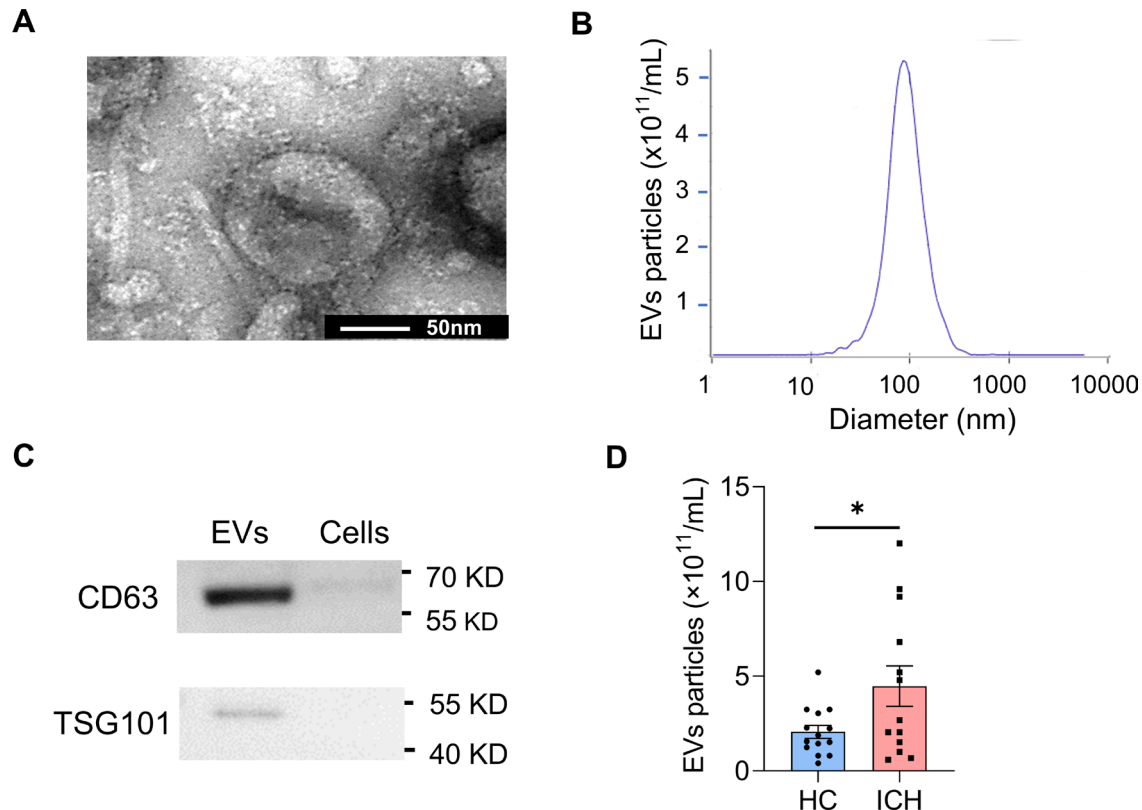
Figure 1 Extracellular vesicles (EVs) are increased in plasma of patients with intracerebral haemorrhage (ICH). (A) Transmission electron micrographs (TEM) image indicating EVs morphology and the size of the EVs. Scale bar=50 nm. (B) Nanoparticle tracking analysis (NTA) results depicting the dimensional distribution of isolated EVs. (C) Western blot analysis of EV-positive markers, including CD63 (cluster of differentiation 63) and TSG101 (tumour susceptibility gene 101). 293 T cells were used as a control. (D) Analysis of concentrations in ICH patients and in healthy controls (HC) using NTA, n=14 in HC and n=13 in ICH patients. *$p<0.05$ by the two-tailed unpaired Student's t-test and data are presented as mean±SEM.

Isolation and characteristics of EVs of ICH patients' plasma

We employed TEM, nanoparticle tracking analysis (NTA) and western blotting to confirm the presence of extracted EVs. TEM revealed the cap-shaped morphology of the vesicles (figure 1A). Analysis by NTA demonstrated that the EVs had a typical diameter ranging from 50 to 200 nm, with a peak at 94 nm (figure 1B), indicating their classification as EVs. Western blotting confirmed the expression of membrane-specific markers for EVs, including cluster of differentiation 63 (CD63) and tumour susceptibility gene 101 protein (TSG101) (figure 1C). Furthermore, the concentration of EVs was significantly higher in the plasma compared with healthy controls (p=0.035) (figure 1D).

Analysis of quantitative proteomics comparison of ICH and control in plasma EVs

We conducted proteomic profiling analysis on 60 samples from ICH and control cohorts, identifying a total of 4994 proteins. Among these, 4509 proteins were detected in both groups, while 250 proteins were unique to the control group and 235 proteins were unique to the ICH group (figure 2A). Within the identified proteins, 49 proteins showed significant upregulation and 12 proteins displayed significant downregulation in the ICH group compared

with the control group (determined by p<0.05 and log2 fold change threshold >1 or <−1; figure 2B; online supplemental tables 3 and 4). The volcano plot illustrates the distribution of all common proteins along with the regulated ones (figure 2C), while the top 10 upregulated and top 5 downregulated DEPs are depicted in figure 2D. Upregulated proteins include inflammation-regulatory proteins such as SAA1, peptidyl-prolyl cis-trans isomerase (FKBP1A), filamin-A (FLN-α) and synaptosomal-associated protein 23 (SNAP23), as well as vessel and neuron regeneration proteins like angiogenin (ANG), brain-specific angiogenesis inhibitor 1-associated protein 2 (BAIAP2) and thymosin beta 4x-linked (TMSB4X), along with blood clotting-related proteins such as alpha-enolase (ENO1) and lectin. Conversely, downregulated proteins include anti-inflammatory proteins like fetuin B and blood vessel regeneration protein thrombospondin 4 (THBS4) (figure 2E). Notably, SAA1 emerged as one of the most abundant proteins in EVs isolated from ICH patients compared with healthy controls (figure 2E).

KEGG pathway enrichment analysis based on DEPs revealed a concentration of proteins involved in regulating the actin cytoskeleton, focal adhesion and adherent junction, suggesting a response of EVs to this pathological
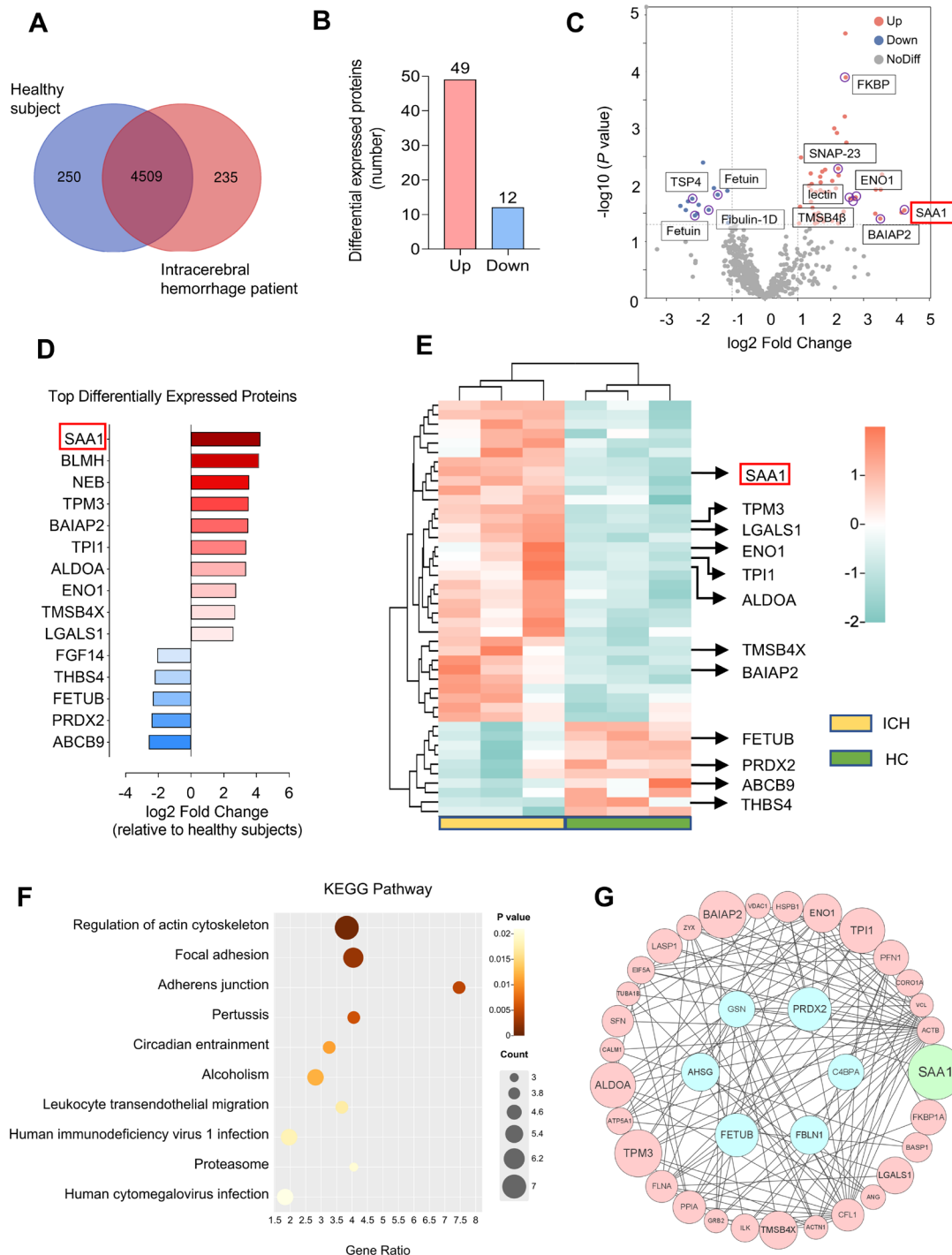
Figure 2 Proteomics profiling of extracellular vesicles isolated from plasma of ICH patients. (A, B) Mass spectrometry (MS) analysis of proteins in extracellular vesicles from 30 ICH patients and 30 healthy subjects. (A) Venn diagram depicting the number of the proteins that were differentially identified between the control and ICH groups. (B) Bar graph illustrating the significantly exchanged proteins as compared with the healthy subjects. p<0.05 and fold change>2. (C) Volcano plot displaying the differentially expressed proteins in ICH patients. Red dots represent significantly upregulated proteins, while blue dots indicate the significantly downregulated proteins as compared with the healthy subjects. The x-axis represents the fold change, and the y-axis shows the p value. (D) Bar graph representing the top altered proteins based on fold change. (E) Hierarchical heat map of extracellular vesicle proteomes, highlighting proteins with fold change >2 and p<0.05 in ICH patients as compared with controls. (F) Functional classification using Kyoto encyclopaedia of genes and genomes (KEGG) revealing the most typical pathway for upregulated proteins in ICH patients as compared with healthy controls. Circle size represents the number of proteins in each pathway and colour indicates p value. Gene ratio is shown on the x-axis. (G) Protein–protein interaction regulation network of significant proteins in the ICH group. Downregulated proteins are at the centre, while the upregulated proteins surround them. Circle size denotes the fold change and lines indicate relationships between proteins. ICH, intracerebral haemorrhage.

process in haemorrhage (figure 2F). GO analysis highlighted significant enrichment across molecular function, cellular component and biological process categories. The top three enriched biological processes were platelet aggregation, actin cytoskeleton organisation and actin filament organisation. Regarding cellular components, the proteins were predominantly associated with focal adhesion, cytosol and cytoplasm. Molecular function classification identified most proteins as actin filament binding, protein binding and actin-binding (online supplemental figure 1A–C). These findings collectively indicate a close association between EVs and cell adhesion, cytoskeletal dynamics and haemostasis, suggesting a biphasic effect of EVs in cerebral haemorrhage. Furthermore, analysis of the PPI network of all these proteins reveals multifaceted protein interactions with SAA1 serving as a hub (figure 2G).

A portion of the upregulated proteins was further validated by ELISA. Enolase (ENO1) showed upregulation in EVs (online supplemental figure 2A) and downregulation in plasma (online supplemental figure 2B). Thymosin beta 4 (TMSB4X), filamin-α (FLN-α) and growth factor receptor-bound protein-2 (Grb2) demonstrated elevated levels in plasma during ICH (online supplemental figure 2D–F), although not significantly in EVs (online supplemental figure 2C). Angiogenin (ANG)

shows no significant change in both plasma and EVs (online supplemental figure 2G,H).

SAA1 promotes microglia-driven proinflammation and leucocyte infiltration in ICH mice

Protein analysis revealed a significant elevation in the level of SAA1 both in EVs and plasma of ICH patients (figure 3A,B). Although no correlation was found between SAA1 level and haemorrhage lesion volume or NIHSS score, a notable correlation emerged between EVs bearing SAA1 and inflammation parameters, including the number of neutrophils (p=0.042) and leucocytes (p=0.038) (figure 3C–H), suggesting a potential link between SAA1 and post-ICH brain inflammation.

The impact of SAA1 on the brain was assessed by administering various doses of exogenous SAA1 or a control vehicle into the basal ganglia region of mice (figure 4A). Results revealed that increased levels of SAA1 (vehicle, 83 ng, 250 ng and 750 ng per mouse) correlated with augmented numbers of microglia and astrocytes (figure 4B–E, online supplemental figure 3) on day 3 postinjection. Annexin V-positive microglia and its subtype remain stable, which indicates that SAA1 likely does not result in a decrease in cell death and apoptosis (p=0.768) (online supplemental figure 4A,B). This suggests that exogenous SAA1 can stimulate the
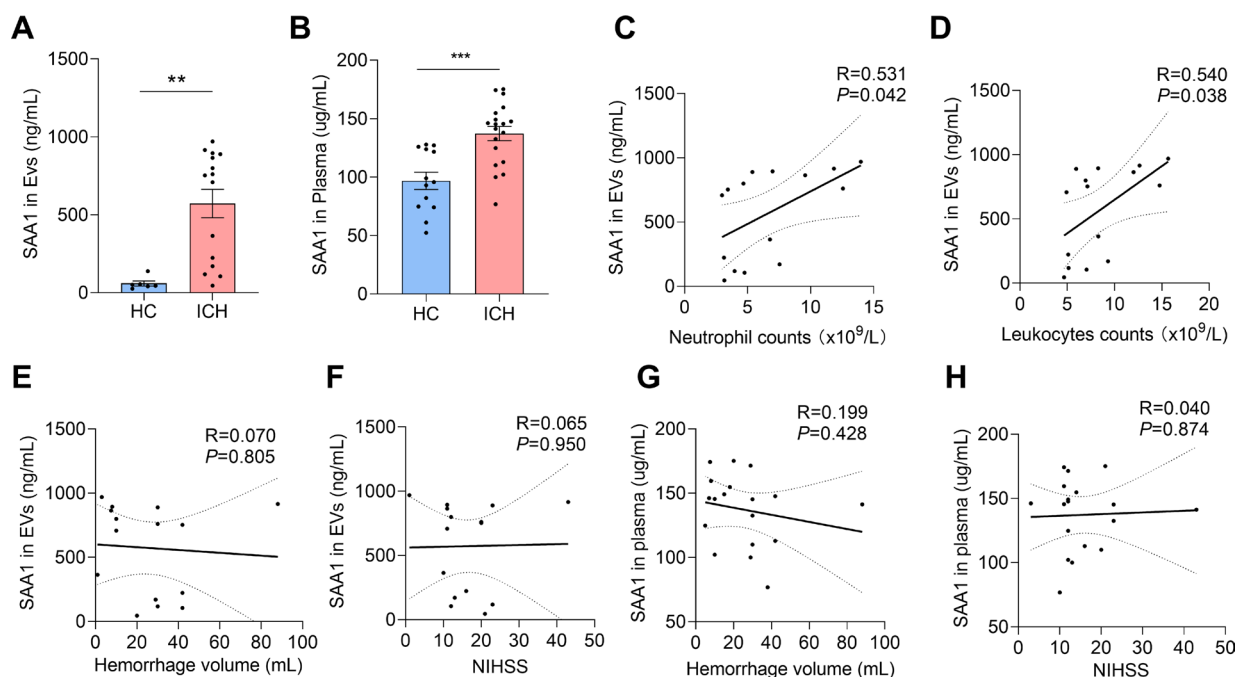

Figure 3 Human serum amyloid A1 (SAA1) protein levels in plasma and extracellular vesicles correlated (EVs) with clinical and laboratory assessments. (A, B) Bar graph indicating the concentration of SAA1 protein in both EVs and plasma for the ICH group and the healthy controls group. Unit: ng/mL in EVs and µg/mL in plasma. **p<0.01, ***p<0.001 by the two-tailed unpaired Student's t-test and data are presented as means±SEM. (A) n=6, 15 in the control and ICH group, (B) n=13, 19 in the control and the ICH group. (C, D) Linear dependence graph revealing the relationship between neutrophils or leucocytes and the SAA1 protein in EVs (n=15). Correlation was analysed by spearman correlation analysis and the dashed line indicates the 95% CI. (E–H) Correlation analysis between the EVs-derived, plasma-derived SAA1 levels and the clinical assessments, including NIHSS and haemorrhage volume, through a linear dependence graph (n=15). Correlation was analysed by spearman correlation analysis and the dashed line indicates the 95% CI. ICH, intracerebral haemorrhage; NIHSS, National Institutes of Health Stroke Scale.
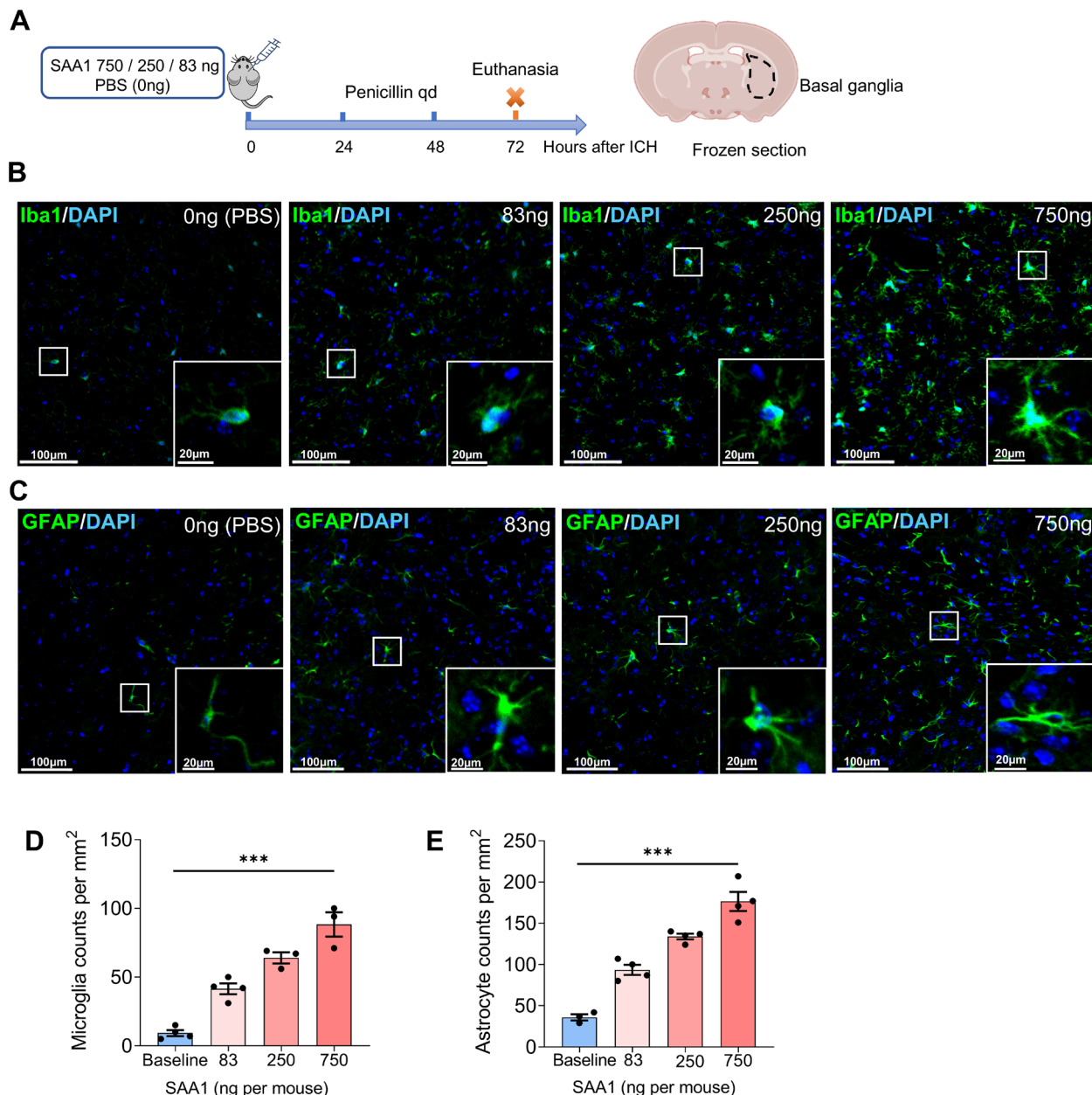
Figure 4 Exogenous SAA1 upregulates the cell counts of microglia and astrocytes. (A) Schematic representation of exogenous SAA1 inserting into the basal ganglia region at varying dosages (750 ng, 250 ng, 83 ng and 0 ng). Images of immunostaining of microglia and astrocyte activation on day three are provided. (B, D) Images of immunostaining (B) and quantification (D) of microglia (stained by a specific marker, Iba1) around the ipsilateral basal ganglia region at different doses of exogenous SAA1. Microglia counts per mm^2: 9.3±2.2, 41.5±3.9, 64.0±4.0, 88.3±8.8 for 0 ng, 83 ng, 250 ng, and 750 ng, respectively. (C, E) Images of immunostaining of GFAP (glial fibrillar acidic protein, known as the astrocyte active marker) representing astrocytes (C) and quantification of astrocytes (E) at different doses of exogenous SAA1 in the ipsilateral basal ganglia region. Astrocyte counts per mm^2: 36.0±3.8, 93.5±6.1, 134.0±3.5, 176.5±11.6 for 0 ng, 83 ng, 250 ng, and 750 ng, respectively. Scale bars=100 μm, inset scale bars=20 μm, n=4 in each group. ***p<0.001 by the Kruskal-Wallis test. Data are presented as means±SEM.

increasing microglia and astrocytes, potentially contributing to post-ICH neuroinflammation. Following induction of ICH, plasma SAA1 levels showed a rise in mice compared with the sham group, as depicted in figure 5A. Treatment with a neutralising anti-SAA1 monoclonal antibody (mAb) via tail vein injection significantly for blocking SAA1 resulted in the increased count of CD206$^+$ microglia (CD45^{int}CD11b$^+$CD206$^+$) on day 1 and day 3, and decreased CD86$^+$ microglia (CD45^{int}CD11b$^+$CD86$^+$)

on day 3 compared with the IgG control (figure 5B–D). However, the total number of microglia remained largely unaffected (figure 5D).

On blocking SAA1 protein, we also observed a decrease in the number of leucocytes, including neutrophils (CD45^{high}Ly6G$^+$), CD8$^+$ T lymphocytes (CD45^{high}CD3$^+$CD8$^+$) and B lymphocytes (CD45^{high}CD19$^+$CD3$^-$) in the brain on day 3 after ICH (figure 5E). This suggests that SAA1 may play a role in neuroinflammation through
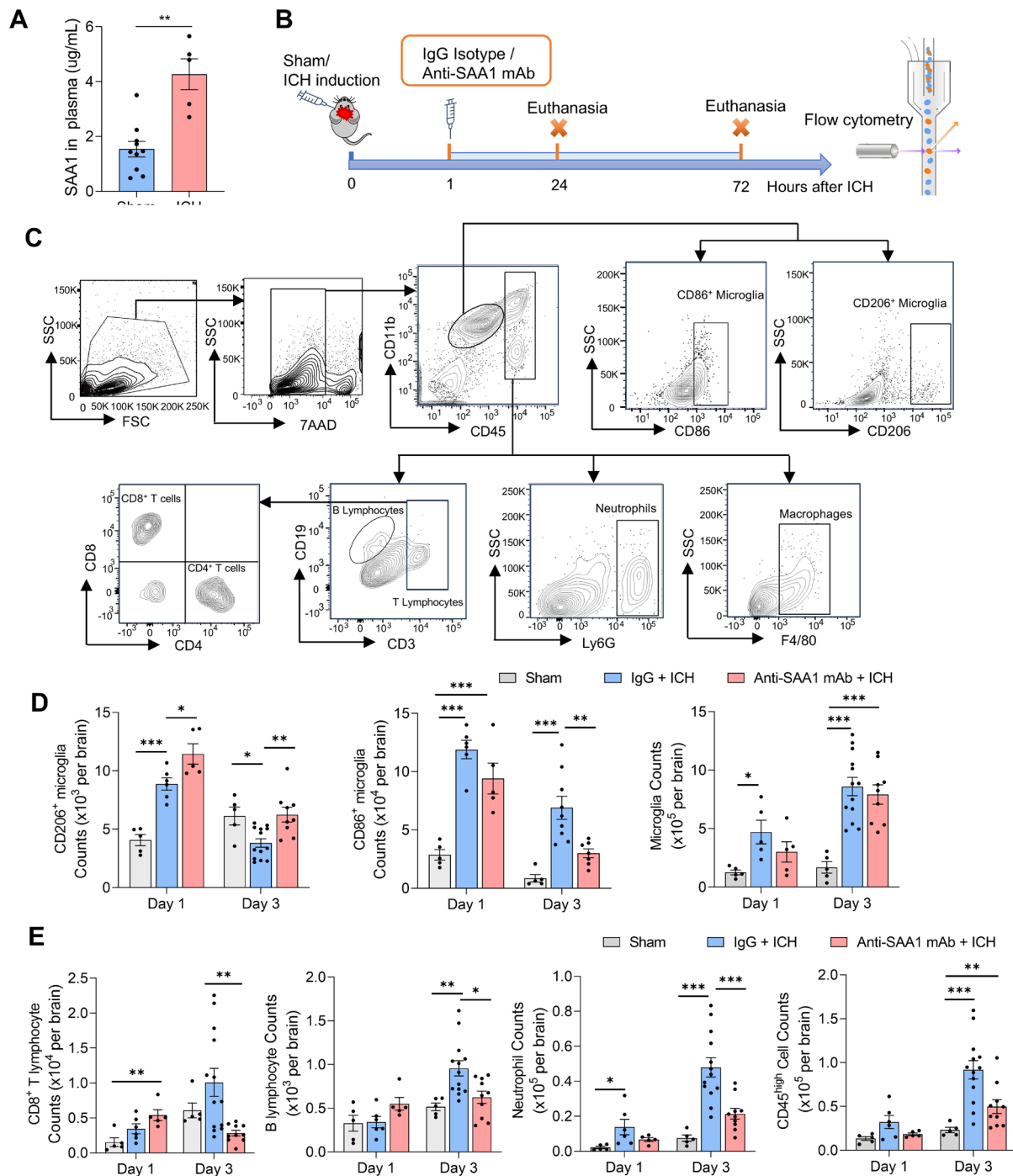
Figure 5 Blocking SAA1 promotes microglia reactivity and leucocyte infiltration. (A) Bar graph indicating the elevation of plasma SAA1 levels in ICH mice as compared with the sham group. n=5 mice in the ICH group and n=10 mice in the sham group. **p<0.01 by two-tailed unpaired Student's t-test. (B) Schematic diagram depicting intracerebral haemorrhage induction followed by intravenous administration of anti-SAA1 mAb or IgG 1 hour later. Immune cell populations were assessed using flow cytometry on days 1 and 3 post-ICH initiation. (C) Flow cytometry gating strategy depicting immune cell populations in mice brain treated with anti-SAA1 antibody or IgG on days 1 and day three post-ICH induction. The graph illustrates CD45^high leucocytes, including CD3+CD19− T lymphocytes and its subtypes: CD4+CD8− T and CD4−CD8+ T lymphocytes, CD3−CD19+ B lymphocytes, CD11b+Ly6G+ neutrophils, and CD11b+F4/80+ macrophages. It also illustrates CD45^int CD11b+microglia, including its subtypes: CD86+ microglia and CD206+ microglia. All gates were set using fluorescence-minus-one (FMO) controls. (D) Bar graph indicates the number of microglia and their subtypes in ICH mice with anti-SAA1 antibody or IgG treatment from days 1 to 3. (E) Bar graph shows major brain infiltrated leucocytes, involving CD8+ T lymphocytes, B lymphocytes, and neutrophils in ICH mice with anti-SAA1 antibody or IgG treatment from days 1 to 3. Int, intermediate. n=5, 6, 5 on day 1 and n=5, 13, 10 on day 3 for sham, IgG and mAb group. n=5, 9, 7 on day 3 for CD86+ microglia group in sham, IgG and mAb group specially. *p<0.05, **p<0.01, ***p<0.001 by one-way ANOVA and Tukey's test. Data are presented as means±SEM. ANOVA, analysis of variance; ICH, intracerebral haemorrhage.
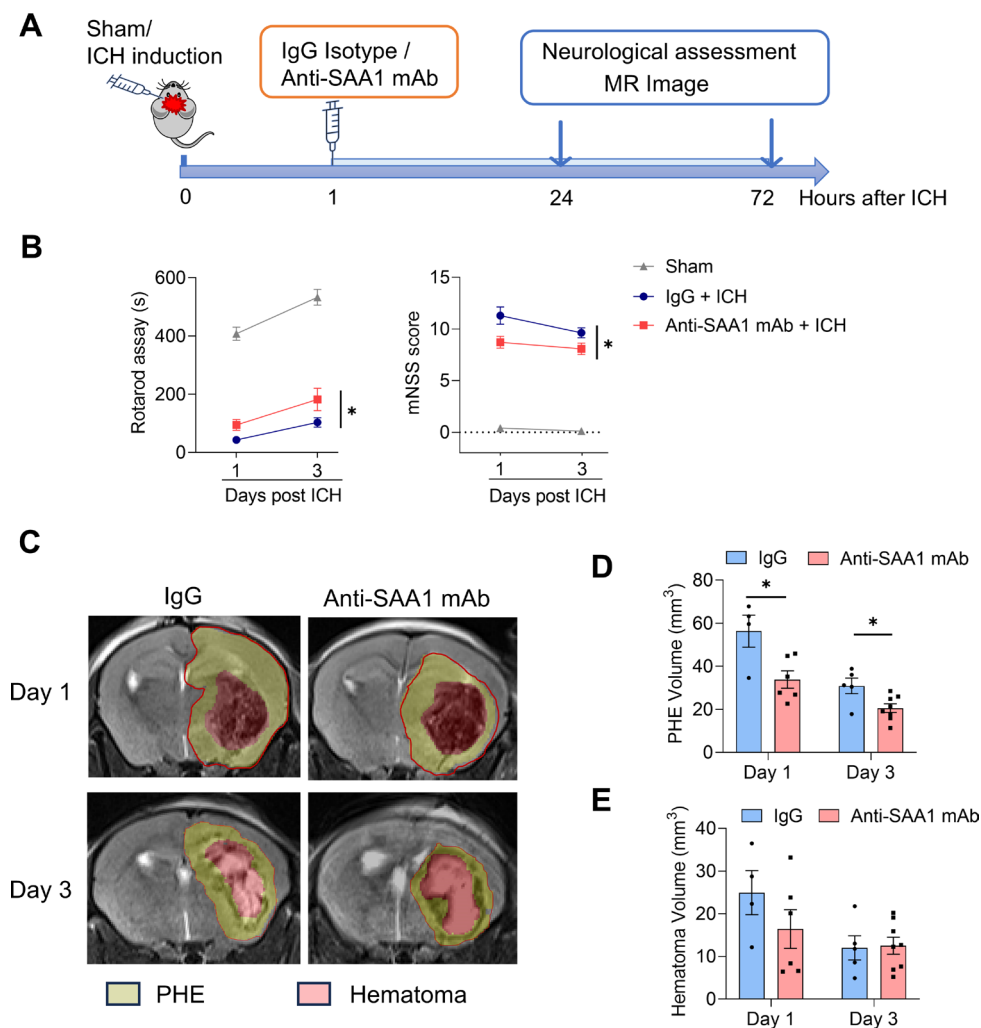
Figure 6 Anti-SAA1 mAb administration alleviates brain injury in mice with ICH. (A) Schematic diagram illustrating the ICH followed by intravenous injection of anti-SAA1 mAb or IgG 1 hour later. Subsequently, mice underwent MRI and neurological evaluations on days 1 and 3 after ICH induction. (B) Neurological scores of the sham group and the ICH group treated with anti-SAA1 mAb or IgG on day 1 and day 3. The modified Neurological Severity Score (mNSS) and rotarod test were used to measure the neurological deficit. n=6, 12, 7 for sham, IgG and mAb group. *p<0.05 by two-way ANOVA. (C) MRI of lesion volume (red) and perihaemorrhagic oedema (PHE) volume (yellow) on day 1 and day 3 post-ICH. (D, E) Quantification of lesion volume and PHE volume using the MRI. n=4, 6 for IgG and mAb group on day 1, n=5, 8 for IgG and mAb group on day 3. *p<0.05 by two-tailed unpaired Student's t-test. Data are presented as means±SEM. ANOVA, analysis of variance; ICH, intracerebral haemorrhage.

increasing number of immune cells at the acute phase, particularly on day 3. Other immune cells showed no significant changes compared with the vehicle control group (online supplemental figure 4C).

Inhabitation of SAA1 relief the brain injury after ICH

We investigated the effects of SAA1 on neurological deficits and brain oedema following ICH (figure 6A). Our findings indicate that neutralising SAA1 improved neurological outcomes on days 1 and 3 after ICH induction, as observed through the rotarod and mNSS scores compared with the IgG group (p=0.018, p=0.029) (figure 6B). Additionally, MRI demonstrated a reduction in perihaematomal oedema volume with anti-SAA1 mAb treatment on both day 1 and day 3 (p=0.019, p=0.020) (figure 6C,D), while the haematoma volume remained unchanged

(figure 6E). These results suggest that blocking SAA1 mitigates neurological deficits and brain oedema in ICH mice.

DISCUSSION

In this study, we used proteomics to demonstrate that EVs from ICH patients exhibited enrichment with SAA1. This enrichment coincided with increased infiltration of immune cell subsets and modulation of microglial reactivity. Blocking SAA1 with mAb mitigated neurological deficits and brain oedema. Our findings underscore the potential of SAA1 from EVs as a biomarker for the proinflammatory response in ICH. Additionally, it may serve as a significant contributor to poststroke neuroinflammation (online supplemental figure 5).

To date, limited proteomics research has focused on screening proteins in blood-derived EVs in stroke, particularly concerning cognitive impairment and the risk of future attacks.[28–30] Prior studies have analysed EVs in a murine model of ICH, comparing differences between acute and chronic phases with a sham group.[12] Our investigation builds on this research by examining EVs in human blood, revealing protein profiles that could aid in identifying stroke biomarkers and therapeutic targets.

EVs play a crucial role in transmitting specific proteins across the BBB, allowing their detection in peripheral fluids during haemorrhage. These vesicles harbour valuable information concerning dysfunctional cells and the associated pathological processes.[31–33] During cerebral haemorrhage, EVs exhibit a dual role in inflammation: they stabilise the BBB while also facilitating the entry of circulating neutrophils into the brain.[9–11] Our study reveals that SAA1, highly abundant in EVs, exacerbates brain inflammation in mice with ICH.

SAA1, an acute-phase protein primarily synthesised by hepatocytes, undergoes upregulation in response to inflammation or stress.[34 35] In various pathological conditions, SAA1 has emerged as a potential prognostic marker for adverse outcomes and increased mortality across different stroke subtypes.[36 37] Furthermore, SAA1 levels have shown correlations with inflammatory processes and infection. Patients who subsequently develop infections after a cerebrovascular event exhibit significant rises in SAA1 levels, paralleling elevations in white cell counts and C reactive protein levels.[35 38]

Previous studies have highlighted the role of SAA1 in poststroke neuroinflammation through its stimulation of microglia.[39] In vitro investigations have elucidated that the SAA1 protein induces the upregulation of interleukin-1 (IL-1) cytokine production in microglia via the Nod-like receptor protein 3 (NLRP3) and caspase-1 pathway, thereby amplifying the proinflammatory cascade associated with ischaemic stroke.[39 40] These findings imply a potential involvement of SAA1 in inflammation via the NLRP3 pathway in ICH. Moreover, experimental autoimmune encephalomyelitis models have demonstrated that SAA1 significantly enhances the differentiation of Th17 cells, consequently leading to increased SAA1 expression in the brain.[41] Additionally, SAA1 exerts notable effects on various immune cells, including neutrophils and macrophages, highlighting its crucial role in modulating immune responses.[34] Considering the implications of these studies, further investigation into SAA1 inhibition holds promise for mitigating inflammation following induced ICH.

This study possesses certain limitations. The small sample size in both the discovery and validation cohorts underscores the necessity of confirming the findings in a larger cohort. The animal models used in this study were also relatively young (8–10 weeks), while stroke predominantly affects older adults. Considering this age discrepancy, more research should be conducted on ageing mice. Furthermore, the potential involvement of SAA1 from plasma and EVs in inflammation necessitates further investigations to ascertain the protein's source. In addition, although our results revealed a disrupted BBB in the ICH model, there remains a lack of direct evidence of a SAA1 antibody distribution in the brain. Lastly, while our study primarily examines the cellular level in the acute phase, delving deeper into the molecular signalling pathways and its long-term effects is essential for enhancing its clinical applicability.

In summary, our study entails proteomic analysis of EVs from ICH patients, identifying protein markers such as SAA1 linked to post-ICH neuroinflammation. Targeting SAA1-induced neuroinflammation may offer a promising approach for immune modulation in acute-phase ICH patients.

ORCID iD
Wei-Na Jin http://orcid.org/0000-0002-1644-4381

REFERENCES

1 Sheth KN. Spontaneous Intracerebral Hemorrhage. *N Engl J Med* 2022;387:1589–96.
2 Benjamin EJ, Muntner P, Alonso A, *et al*. Heart Disease and Stroke Statistics-2019 Update: A Report From the American Heart Association. *Circulation* 2019;139:e56–528.
3 Hemphill JC 3rd, Greenberg SM, Anderson CS, *et al*. Guidelines for the Management of Spontaneous Intracerebral Hemorrhage: A Guideline for Healthcare Professionals From the American Heart Association/American Stroke Association. *Stroke* 2015;46:2032–60.
4 Nickel W, Rabouille C. Mechanisms of regulated unconventional protein secretion. *Nat Rev Mol Cell Biol* 2009;10:148–55.
5 Lai C-K, Breakefield XO. Role of exosomes/microvesicles in the nervous system and use in emerging therapies. *Front Physiol* 2012;3:228.
6 Liu W, Bai X, Zhang A, *et al*. Role of Exosomes in Central Nervous System Diseases. *Front Mol Neurosci* 2019;12:240.

7 Kalani A, Tyagi A, Tyagi N. Exosomes: mediators of neurodegeneration, neuroprotection and therapeutics. *Mol Neurobiol* 2014;49:590–600.

8 Otero-Ortega L, Laso-García F, Gómez-de Frutos M, *et al*. Role of Exosomes as a Treatment and Potential Biomarker for Stroke. *Transl Stroke Res* 2019;10:241–9.

9 Laso-García F, Casado-Fernández L, Piniella D, *et al*. Circulating extracellular vesicles promote recovery in a preclinical model of intracerebral hemorrhage. *Mol Ther Nucleic Acids* 2023;32:247–62.

10 Li M, Li X, Wang D, *et al*. Inhibition of exosome release augments neuroinflammation following intracerebral hemorrhage. *FASEB J* 2021;35:e21617.

11 Wu X, Liu H, Hu Q, *et al*. Astrocyte-Derived Extracellular Vesicular miR-143-3p Dampens Autophagic Degradation of Endothelial Adhesion Molecules and Promotes Neutrophil Transendothelial Migration after Acute Brain Injury. *Adv Sci (Weinh)* 2024;11:2305339.

12 Laso-García F, Piniella D, Gómez-de Frutos MC, *et al*. Protein content of blood-derived extracellular vesicles: An approach to the pathophysiology of cerebral hemorrhage. *Front Cell Neurosci* 2022;16:1058546.

13 Carandini T, Colombo F, Finardi A, *et al*. Microvesicles: What is the Role in Multiple Sclerosis? *Front Neurol* 2015;6:111.

14 Wheway J, Latham SL, Combes V, *et al*. Endothelial microparticles interact with and support the proliferation of T cells. *J Immunol* 2014;193:3378–87.

15 Sáenz-Cuesta M, Osorio-Querejeta I, Otaegui D. Extracellular Vesicles in Multiple Sclerosis: What are They Telling Us? *Front Cell Neurosci* 2014;8:100.

16 Lombardi M, Parolisi R, Scaroni F, *et al*. Detrimental and protective action of microglial extracellular vesicles on myelin lesions: astrocyte involvement in remyelination failure. *Acta Neuropathol* 2019;138:987–1012.

17 Huang L-H, Rau C-S, Wu S-C, *et al*. Identification and characterization of hADSC-derived exosome proteins from different isolation methods. *J Cell Mol Med* 2021;25:7436–50.

18 Mincheva-Nilsson L, Baranov V, Nagaeva O, *et al*. Isolation and Characterization of Exosomes from Cultures of Tissue Explants and Cell Lines. *Curr Protoc Immunol* 2016;115:14.

19 Cox J, Mann M. MaxQuant enables high peptide identification rates, individualized p.p.b.-range mass accuracies and proteome-wide protein quantification. *Nat Biotechnol* 2008;26:1367–72.

20 Choi M, Chang C-Y, Clough T, *et al*. MSstats: an R package for statistical analysis of quantitative mass spectrometry-based proteomic experiments. *Bioinformatics* 2014;30:2524–6.

21 Yu G, Wang L-G, Han Y, *et al*. clusterProfiler: an R package for comparing biological themes among gene clusters. *OMICS* 2012;16:284–7.

22 Li Z, Li Y, Han J, *et al*. Formyl peptide receptor 1 signaling potentiates inflammatory brain injury. *Sci Transl Med* 2021;13:eabe9890.

23 Shi SX, Xiu Y, Li Y, *et al*. CD4⁺ T cells aggravate hemorrhagic brain injury. *Sci Adv* 2023;9:eabq0712.

24 Smole U, Gour N, Phelan J, *et al*. Serum amyloid A is a soluble pattern recognition receptor that drives type 2 immunity. *Nat Immunol* 2020;21:756–65.

25 Liu Q, Sanai N, Jin W-N, *et al*. Neural stem cells sustain natural killer cells that dictate recovery from brain inflammation. *Nat Neurosci* 2016;19:243–52.

26 Shi SX, Li Y-J, Shi K, *et al*. IL (Interleukin)-15 Bridges Astrocyte-Microglia Crosstalk and Exacerbates Brain Injury Following Intracerebral Hemorrhage. *Stroke* 2020;51:967–74.

27 Hua Y, Schallert T, Keep RF, *et al*. Behavioral tests after intracerebral hemorrhage in the rat. *Stroke* 2002;33:2478–84.

28 Datta A, Chen C, Gao Y-G, *et al*. Quantitative Proteomics of Medium-Sized Extracellular Vesicle-Enriched Plasma of Lacunar Infarction for the Discovery of Prognostic Biomarkers. *Int J Mol Sci* 2022;23:11670.

29 Mitaki S, Wada Y, Sheikh AM, *et al*. Proteomic analysis of extracellular vesicles enriched serum associated with future ischemic stroke. *Sci Rep* 2021;11:24024.

30 Qi B, Kong L, Lai X, *et al*. Plasma exosome proteomics reveals the pathogenesis mechanism of post-stroke cognitive impairment. *Aging (Albany NY)* 2023;15:4334–62.

31 Lee EC, Ha TW, Lee D-H, *et al*. Utility of Exosomes in Ischemic and Hemorrhagic Stroke Diagnosis and Treatment. *Int J Mol Sci* 2022;23:8367.

32 Vinaiphat A, Sze SK. Proteomics for comprehensive characterization of extracellular vesicles in neurodegenerative disease. *Exp Neurol* 2022;355:114149.

33 Marostica G, Gelbter S, Gironi M, *et al*. Extracellular Vesicles in Neuroinflammation. *Front Cell Dev Biol* 2020;8:623039.

34 Chen R, Chen Q, Zheng J, *et al*. Serum amyloid protein A in inflammatory bowel disease: from bench to bedside. *Cell Death Discov* 2023;9:154.

35 Schweizer J, Bustamante A, Lapierre-Fétaud V, *et al*. SAA (Serum Amyloid A): A Novel Predictor of Stroke-Associated Infections. *Stroke* 2020;51:3523–30.

36 Huangfu X-Q, Wang L-G, Le Z-D, *et al*. Utility of serum amyloid A as a potential prognostic biomarker of acute primary basal ganglia hemorrhage. *Clin Chim Acta* 2020;505:43–8.

37 Chang Q, Li Y, Xue M, *et al*. Serum amyloid A is a potential predictor of prognosis in acute ischemic stroke patients after intravenous thrombolysis. *Front Neurol* 2023;14:1219604.

38 Azurmendi L, Degos V, Tiberti N, *et al*. Measuring Serum Amyloid A for Infection Prediction in Aneurysmal Subarachnoid Hemorrhage. *J Proteome Res* 2015;14:3948–56.

39 Yu J, Zhu H, Taheri S, *et al*. Serum Amyloid A-Mediated Inflammasome Activation of Microglial Cells in Cerebral Ischemia. *J Neurosci* 2019;39:9465–76.

40 Losey P, Ladds E, Laprais M, *et al*. The role of PPAR activation during the systemic response to brain injury. *J Neuroinflammation* 2015;12:99.

41 Lee J-Y, Hall JA, Kroehling L, *et al*. Serum Amyloid A Proteins Induce Pathogenic Th17 Cells and Promote Inflammatory Disease. *Cell* 2020;180:79–91.